Hindawi
Advances in Civil Engineering
Volume 2019, Article ID 4970269, 16 pages
https://doi.org/10.1155/2019/4970269

Research Article

Influence of Small, Clear Distance Cross-Tunnel Blasting Excavation on Existing Tunnel below

Baofu Duan,[1,2] Weizeng Gong,[1,2] Guoshan Ta,[1,2] Xuxu Yang,[1,2] and Xuewei Zhang[1,2]

[1]*Key Laboratory of Civil Engineering Disaster Prevention and Mitigation, Shandong University of Science and Technology, Qingdao, Shandong 266590, China*
[2]*College of Civil Engineering and Architecture, Shandong University of Science and Technology, Qingdao, Shandong 266590, China*

Correspondence should be addressed to Guoshan Ta; taguoshan0324@163.com

Received 22 April 2019; Revised 6 August 2019; Accepted 9 September 2019; Published 31 October 2019

Academic Editor: Hugo Rodrigues

The vibration effect generated during tunnel excavation can influence or damage adjacent tunnels. Studying and controlling the blasting vibration effect has important theoretical and practical significance, especially for new tunnels. This paper takes the tunnel project of Gao Jiu Lu-Jia Hua Cross Tunnel in Chongqing as the research background and assesses the blasting vibration influence in the up-down cross-tunnel. Onsite monitoring and numerical simulation were used to analyze peak particle velocity (PPV) changes, stress distribution, and crown settlement during the excavation process of Gao Jiu Lu I Tunnel at Jia Hua Tunnel Left Line in the cross-section. Influence laws of blasting excavation in a small, clear distance cross-tunnel on an existing tunnel below were obtained. Results show that new tunnel blasting vibrations exerted the largest influence on the crown of the existing tunnel below in the cross-section. The maximum tensile stress of the secondary lining of the existing tunnel below was mainly concentrated in the crown area. The maximum compressive stress during excavation was concentrated in the crown foot, and the stress value was less than the tensile and compressive strength of the concrete. The loosening of the surrounding rock from blasting excavation of the new tunnel caused secondary settlement of the existing tunnel crown below. The cumulative settlement value at the cross-section of the two tunnels was the largest. With an increase in axial distance from the cross-section of the existing tunnel crown, the settlement value gradually declined and became stable. These research results have reference value for the construction of a small, clear distance cross-tunnel and provide theoretical guidance for similar tunnel excavation projects in the future.

1. Introduction

During construction projects, topographic and geological constraints often cause two parallel tunnels to be excavated in parallel; alternatively, a new tunnel can be built near the existing tunnel. The blasting excavation of the construction tunnel may cause nearby damage to the surrounding tunnel rock, thereby affecting surrounding rock stability in the existing tunnel, jeopardizing tunnel safety, and hindering safe construction of the new tunnel. The safety influence of a newly built tunnel on the structure of the adjacent existing tunnel mainly manifests through two aspects: blasting vibration and stress redistribution caused by tunnel excavation.

To evaluate the blasting vibration effect of tunneling, scholars have conducted extensive research on the propagation law of blasting vibration waves and the influence on underground opening through blasting vibration in onsite and indoor tests [1–5]. Li et al. [6] proposed a theoretical method to predict underground tunnel behavior considering the peak particle velocity (PPV) and the stress distribution. By case study, the vibration of the adjacent tunnel is mainly controlled by the explosion-induced wave propagation and the maximum radial stress occurs in the adjacent tunnel wall nearest to the charge tunnel. In the study by Zhao et al. [7], based on the blasting vibration velocity and vibration frequency, the axial and radial blasting vibration velocity distribution of the existing tunnel under the influence of the explosion vibration of adjacent subway tunnels is studied. The results showed that the numerical simulation can optimize the blasting vibration response of adjacent tunnel blasting excavation to existing

tunnels. Chen et al. [8] studied the effect of blasting excavation disturbance on the surrounding rock damage zone in deep-buried tunnels by means of in-situ rock mass acoustic velocity detection and numerical simulation. The results show that the blasting load and the transient unloading of excavation loads are important factors for the development of the surrounding rock excavation damage zone. Li et al. [9] simulated the dynamic response of the existing tunnel under unloading disturbance using three-dimensional numerical simulation. It was found that the PPV of the unloaded microvibration can be as high as the PPV of the explosion-induced wave. Liang et al. [10] conducted a comprehensive study on the impact of new tunnel blasting vibration on existing railway tunnels in Xinjiang and proved that adjusting the original blasting design and corresponding parameters can effectively reduce the maximum blasting vibration velocity (BVV). In order to study the effects of tunnel blast construction on the surrounding rock and the lining systems of adjacent existing tunnels, Li et al. [11] monitored the vibration of the existing tunnel real time, and the monitoring results showed that the main frequency distributions of the radial, tangential, and vertical vibration of the subway tunnel were significantly different. Yang et al. [12] proposed a three-dimensional numerical model of a new type of prestressed composite lining, which can simulate the structural characteristics and bearing mechanism of the lining. Feldgun et al. [13] proposed a comprehensive approach to examine the effects of explosions on the behavior of nearby infrastructure tunnels, including the use of AUTODYN 12. The effects of microseisms caused by explosions on existing tunnel linings are most likely to occur based on vibrational velocity and dynamic strain. The damaged area is the vault and the side wall. Xia et al. [14] analyzed the damage of surrounding rock and lining systems under different explosive loads and obtained the degree of damage of tunnel surrounding rock linearly with the PPV of existing tunnels and proposed a feasible PPV-based damage control method for different parts of the tunnel. People are also exploring fast and low-cost evaluation methods while gaining an in-depth understanding of tunnel blasting vibration effects. Liang et al. [15] studied the interaction mechanism between existing tunnels and proposed a simplified analysis and evaluation method to better understand and evaluate the impact of cross-tunneling on existing tunnels.

Scholars have begun to grasp the impact of blasting construction on adjacent tunnels by analyzing various tunnel conditions. However, due to the influence of seismic waves generated by excavation blasting on neighboring tunnels, research findings remain immature. At present, for the construction environment with a large excavation surface, high blasting intensity, and frequent earthquakes on the surface and lining, the vibration and stress of the existing tunnel lining during the tunnel blasting excavation process have not been studied. In this paper, based on the Gao Jiu Lu-Jia Hua Cross Tunnel in Chongqing, onsite monitoring measurement and numerical simulation analysis are used to analyze the blasting construction control technology of the up-down cross-tunnel. The blasting excavation of the new tunnel above is examined based on the influence of blasting vibration, stress redistribution, and cumulative crown settlement. The influence law of blasting excavation in a small, clear distance cross-tunnel on the existing tunnel below is obtained. The research results of this paper can predict and control overall and local damage to the existing tunnel below caused by blasting to ensure the safety of the new tunnel construction and provide a theoretical basis and guidance for similar projects in the future.

2. Onsite Monitoring Program and Data Analysis

2.1. Project Overview. Gao Jiu Lu-Jia Hua Up-down Cross Tunnel is a small, clear distance cross-tunnel project at the intersection of Jia Hua Tunnel and Gao Jiu Lu I and J Tunnels on the south-north main Lu in Chongqing. The mileage of Gao Jiu Lu I Tunnel is K0 + 182.9–K0 + 240.7; the mileage of Gao Jiu Lu J Tunnel is K0 + 184.5–K0 + 240.0. The tunnel passed over on the K5 + 882.2–K5 + 892.7 of Jia Hua Tunnel Left Line and Jia Hua Tunnel Right Line is K5 + 854.6–K5 + 864.8, respectively (see Figure 1). The thickness of the minimum residual rock mass between Gao Jiu Lu Tunnel and Jia Hua Tunnel is approximately 0.9 m. The floor of the Gao Jiu Lu Tunnel is thin, and the overlying soil is thick. Gao Jiu Lu Tunnel is a single-hole tunnel with a standard net span of 8.76 m, a design hole measuring 6.6 m high, and a tunnel axis span of 12.45 m. Jia Hua Tunnel is a double-track, double-hole tunnel with a net span of 12.45 m and a height of 7.2 m, and the axes of the tunnel are 43.75 m apart. Compared with Jia Hua Tunnel, Gao Jiu Lu Tunnel is relatively new.

Surface investigation and drilling revealed that the surface layer of this section was mainly quaternary colluvium, alluvium, and miscellaneous fill due to human engineering. The alluvial layers were all distributed on the Jialing River terraces in the north of Jialing Lu with a thickness of 8–20 m. The colluvium was mainly distributed in the area along Jialing Lu and its south, with a thickness of 3–5 m. Miscellaneous fill was not distributed continuously throughout the entire site (thickness of 2–10 m). The underlying bedrock was a continental sedimentary rock of the Shaximiao Formation of the Jurassic Central System. The main lithology could be divided into sandstone, sandy mudstone, and others, and the phase change phenomenon was developed. The weathering at the top was strong; the thickness of the strong weathered layer was 0.5–1.5 m. The surrounding rock of the tunnel site was weakly weathered sandy mudstone, and the uniaxial saturation compressive strength of which was 5–15.0 MPa. It was a soft rock, and the rock body integrity was poor. The buried depth of the tunnel, which was deep, was 17–49 m. The thickness of its roof rock was 18–36 m. The surrounding rock was Grade IV, cracks had not developed, and the layer was micropermeable. The geological picture of palm face in blasting excavation of ramp I of Gaojiu road is shown in Figure 2. The cross-section of the section was 20°–25°, and the section was steep, reaching 50°–60°. The thickness of the residual rock mass between tunnels was 1–2.5 m. The tunnel lining structure was designed according to NATM and used a composite lining structure. C30 concrete was used for the primary branch with a spray thickness of 20 cm, and C30 concrete with a thickness of 40 cm was used for the secondary lining.

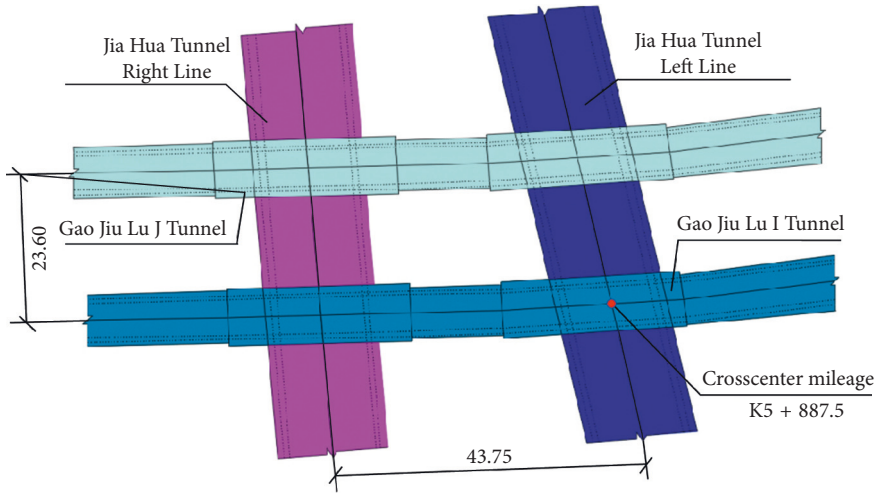

Figure 1: Crossover view of two tunnels (unit: m).

2.2. Tunnel Blasting Vibration Monitoring. A reasonable safety control range must be determined during blasting construction of a new tunnel. The vibration response of the existing tunnel below must also be monitored to ensure the safety of the existing tunnel [16–19]. This study used onsite monitoring of the existing tunnel in the cross-section. The blasting vibration monitoring system employed the Model 891 vibrometer produced by the Institute of Engineering Mechanics, China Seismological Bureau. The vibrometer was mainly used to measure the pulsation or engineering vibration of the ground and structures. Each vibrometer included six 891 vibration eliminators and one 891 six-wire amp. The vibration pickup was equipped with three speeds: medium speed, large speed, and acceleration. The amplifier included the functions of amplification, integration, filtering, and impedance transformation. As needed, the microtoggle switch on the vibration pickup and the parameter selection switch on the amplifier could be selected to choose the corresponding gear; the acceleration, speed, and displacement parameters of the measured point could thus be obtained. The maximum range of the acceleration of the vibration pickup could reach 20 m/s^2. The resolution of the 891-type amplifier after mating was 1×10^{-5}, and the vibration effect of blasting on the city wall could be measured completely. The acquisition and analysis system employed DASP (Data Acquisition and Signal Processing-V11) software, a complete set of signal oscillography and real-time spectrum analysis. It integrates the most commonly used dynamic analysis testing and analysis methods, and the output can take various forms.

The minimum clear distance between the Gao Jiu Lu I Tunnel and Jia Hua Tunnel Left Line was 0.9 m, and the minimum clear distance between Gao Jiu Lu J Tunnel and Jia Hua Tunnel Right Line was 1.6 m. This article only selected the most representative cross-section, namely, the minimum clear distance of Gao Jiu Lu I Tunnel and Jia Hua Tunnel Left Line cross-section. Gao Jiu Lu I Tunnel excavation used the upper and lower long-step method; the excavation height of the upper bench was 4 m, and that of the lower bench was 2.6 m. When the upper step was excavated and the floor thickness was equal to or greater than 4 m, blasting was conducted at a depth of 1.0 m per cycle. When the floor thickness was less than 4 m, blasting was conducted at a depth of 0.5 m per cycle. When the lower bench was excavated and the floor thickness was equal to or greater than 4 m, the excavation was conducted at a blasting depth of 0.5 m per cycle. When the floor thickness was less than 4 m, mechanical crushing was used in combination with manual excavation. The specific excavation method is shown in Figure 3.

During the excavation of Gao Jiu Lu I Tunnel, the excavation section on the upper bench was large and blasting was still used when passing through Jia Hua Tunnel Left Line. Therefore, I Tunnel blasting excavation on the upper bench was selected as the main vibration monitoring object. Measure points were arranged in Jia Hua Tunnel Left Line at the cross-section of the two tunnels, with three measuring points arranged on the surface of the second liner of Jia Hua Tunnel Left Line at K5 + 887.5 miles: A measuring point on the crown, B measuring point on the left arch foot, and C measuring point on the right arch foot. The A measurement point was recorded as the blasting source distance from the measurement point at a horizontal distance of 0 points, see the layout in Figure 3. When the measuring sensor was fixed on the site, an electric drill was used to bore the expansion screw hole on the lining. Using gypsum powder and water as a paste, the sensor was affixed to the surface of the measuring point. Stainless steel clips and expansion screws were used to ensure the sensor could vibrate with the lining. During the installation process, the vertical direction Z was kept as perpendicular to the horizontal plane as possible. The horizontal X direction should be parallel to the tunnel axis, and the horizontal Y direction should be perpendicular to the tunnel wall. To prevent destruction from flying stones while blasting, monitoring instruments and sensors were integrated with iron boxes with expansion screws.

2.3. Vibration Monitoring Data Analysis. Gao Jiu Lu I Tunnel excavation method was arranged symmetrically on

Figure 2: Geological picture of palm face in blasting excavation of ramp I of Gaojiu road.

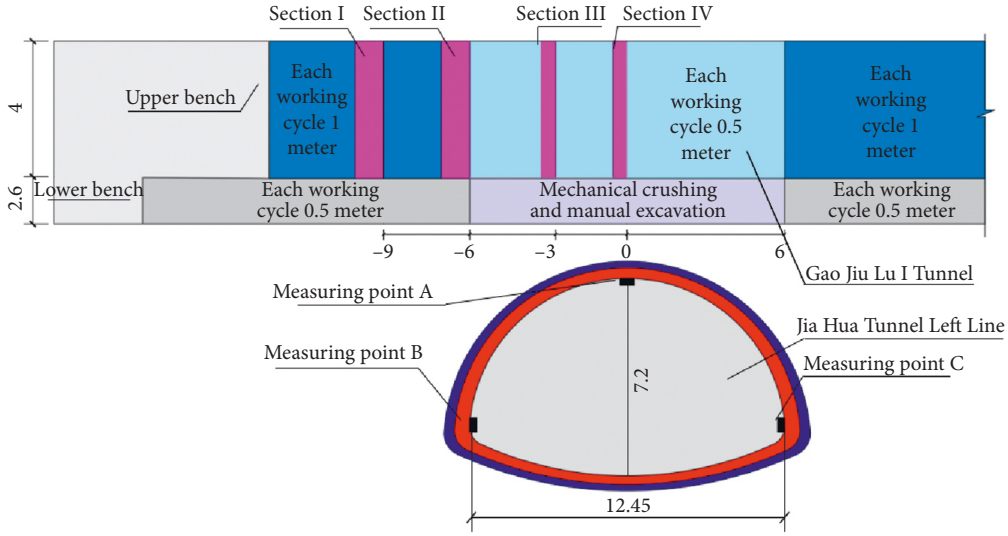

Figure 3: Excavation method of Gao Jiu Lu I Tunnel and layout of measuring points on Jia Hua Tunnel Left Line (unit: m).

each side of Jia Hua Tunnel Left Line, and the blasting excavation vibration on one side was selected for analysis. The blasting excavation was performed from 1 m per cycle to 0.5 m per cycle, and the vibration of each cycle was recorded. Due to space limitations and convenient data analysis, this paper addresses four representative blasting sections along the excavation direction: Section I, Section II, Section III, and Section IV. The horizontal distance from Jia Hua Tunnel Left Line below were 9 m, 6 m, 3 m, and 0 m, respectively. The blasting cycle footage of Sections I and II was 1 m, and the blasting cycle footage of Sections III and IV was 0.5 m. The specific positions are shown in Figure 3. The time-history curves of measured synthetic vibration speed at the three points in Jia Hua Tunnel Left Line A, B, and C during the blasting process of Gao Jiu Lu I Tunnel can be seen in Figures 4~6.

From Figure 4(a), the PPV at Point A of Section I blasting was 6.73 cm/s, the peak time was 0.01 s, the peak acceleration was 38.43 cm/s^2, and the vibration was close to zero at 1.4 s. Figure 4(b) shows that the PPV at Point A of Section II blasting was 8.96 cm/s, the peak time was 0.008 s, the peak acceleration was 62.84 cm/s^2, and the vibration was close to zero at 1.0 s. Figure 4(c) indicates that the PPV at Point A of Section III blasting was 8.25 cm/s, the peak time was 0.007 s, the peak acceleration was 67.38 cm/s^2, and the vibration was close to zero at 1.6 s. Figure 4(d) illustrates that the PPV at Point A of Section IV blasting was 9.48 cm/s, the peak time was 0.005 s, the peak acceleration was 79.23 cm/s^2, and the vibration was close to zero at 0.8 s.

Figure 5(a) shows that the PPV at Point B of Section I blasting was 5.22 cm/s, the peak time was 0.014 s, the peak

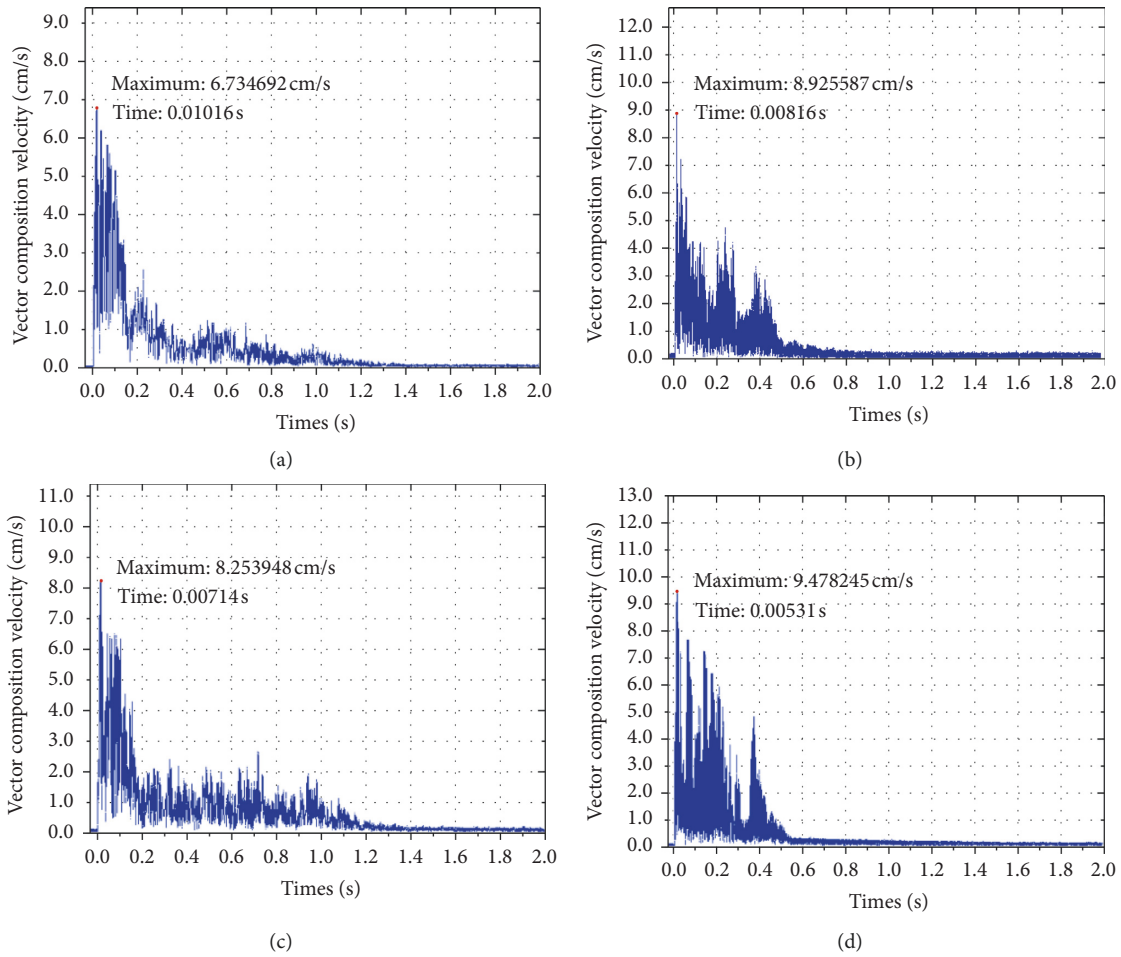

Figure 4: Time-history curve of vibration velocity at Point A during blasting of Section I (a), Section II (b), Section III (c), and Section IV (d).

acceleration was 32.74 cm/s^2, and the vibration was close to zero at 0.6 s. Figure 5(b) displays that the PPV at Point B of Section II blasting was 8.05 cm/s, the peak time was 0.012 s, the peak acceleration was 39.25 cm/s^2, and the vibration was close to zero at 1.0 s. Figure 5(c) illustrates that the PPV at Point B of Section III blasting was 6.57 cm/s, the peak time was 0.01 s, the peak acceleration was 41.57 cm/s^2, and the vibration was close to zero at 0.8 s. In Figure 5(d), the PPV at Point B of Section IV blasting was 5.38 cm/s, the peak time was 0.008 s, the peak acceleration was 71.75 cm/s^2, and the vibration was close to zero at 0.6 s.

In Figure 6(a), the PPV at Point C of Section I blasting was 4.62 cm/s, the peak time was 0.017 s, the peak acceleration was 30.97 cm/s^2, and the vibration was close to zero at 0.6 s. Figure 6(b) shows that the PPV at Point C of Section II blasting was 6.21 cm/s, the peak time was 0.015 s, the peak acceleration was 35.90 cm/s^2, and the vibration was close to zero at 0.4 s. Figure 6(c) indicates that the PPV at Point C of Section III blasting was 5.09 cm/s, the peak time was 0.011 s, the peak acceleration was 41.36 cm/s^2, and the vibration was close to zero at 0.4 s. Figure 6(d) illustrates that the PPV at Point C of Section IV blasting was 5.27 cm/s, the peak time was 0.007 s, the peak acceleration was 42.95 cm/s^2, and the vibration was close to zero at 0.6 s.

The vibration monitoring data of Jia Hua Tunnel during the blasting excavation of Gao Jiu Road are shown in Table 1. By comparing the monitoring data in Table 1, it can be seen that the blasting vibration produced by the blasting excavation of Section IV is the largest, which indicates that the smaller the distance between the upper and lower tunnels, the larger the blasting vibration. That is to say, the blasting vibration of the upper and lower crossing tunnels also conforms to the general blasting vibration law that the vibration speed is inversely proportional to the distance between the blast centers [20, 21]. The peak velocity of the measurement Point A (that is, the location of the tunnel lining dome) is the largest during the blasting process of each section, which indicates that the blasting excavation has the greatest influence on the vault of the existing tunnel. As shown in Table 1, in the four selected blasting sections, the peak acceleration produced by the blasting excavation of Section 4 is the largest, and the peak acceleration of the measurement Point A is also the largest in the blasting process of each section. The variation law of the peak acceleration and the peak vibration velocity is the same. When the distance between the explosion source is smaller, the peak value of blasting vibration acceleration is larger, and the vibration velocity fluctuation of the measured points is more

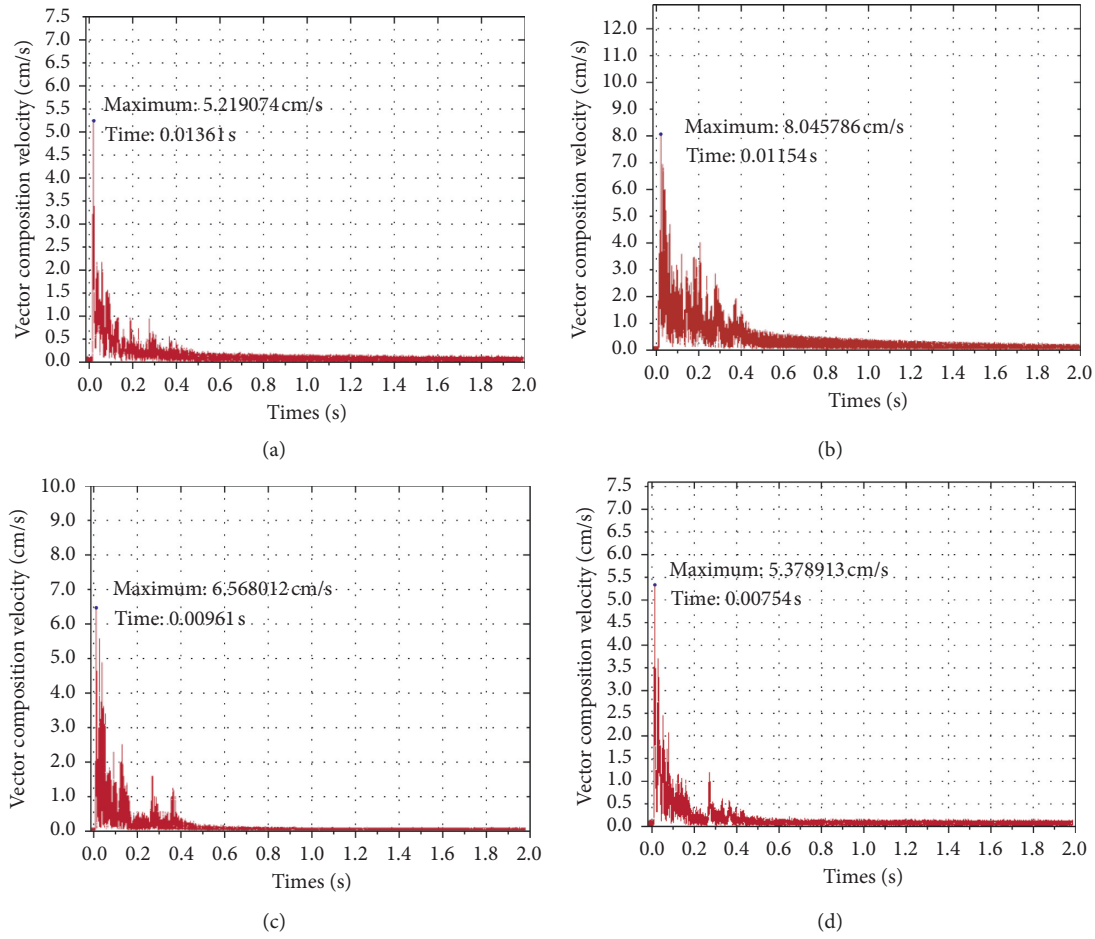

Figure 5: Time-history curve of vibration velocity at Point B during blasting of Section I (a), Section II (b), Section III (c), and Section IV (d).

intense, which indicates that the impact on masonry structure is greater.

At present, the internationally popular safety standards for blasting vibration are based on peak particle velocity or peak particle velocity combined with vibration frequency. In this paper, the measured peak particle velocity is used as the safety criterion to evaluate the existing railway tunnel. At the same time, the vibration acceleration can directly reflect the magnitude of the force, and the acceleration value is used as a reference for safety evaluation. According to the measured data from the cross-section of Gao Jiu Lu I Tunnel and Jia Hua Tunnel Left Line, the maximum vibration speed of the second lining of Jia Hua Tunnel Left Line below during blasting excavation of I Tunnel was 9.48 cm/s. According to China's "Blasting Safety Regulations" (QCR9218-2015), the safety standard for blast tunnel vibration velocity in traffic tunnels is 10–20 cm/s, the maximum acceleration peak value detected in the second lining of Jiahua Tunnel is 79.23 cm/s^2, and the fluctuation range of the peak acceleration is 30–80 cm/s^2. The peak acceleration value is small and will not cause damage. Therefore, the blasting velocity generated by I Tunnel blasting was less than the national control standard.

Gao Jiu Lu I Tunnel blasting excavation affected the second lining of Jia Hua Tunnel Left Line below within the allowable range, and the second lining did not exhibit poor stability or damage. The PPV of vector synthesis at Points A, B, and C is plotted in Figure 7.

Figure 7 shows that the blue, red, and green lines, respectively, represent the peak change lines of the vibration velocity of the four blasting sections at Points A, B, and C. The horizontal distance from Sections I, II, III, and IV is progressively getting shorter and shorter. At Point A (the crown), the peak change rose, fell, and then rose, and at Point B (left arch foot), it rose and then fell twice. The peak change of Point C (right arch foot) rose, fell, and then rose. In the overall comparison of the PPV of the A, B, and, C measuring points, the vibration of Point A was largest, followed Point B, and finally Point C. This pattern suggests that the blasting excavation of the new tunnel had the greatest impact on the vibration of the crown of the existing tunnels below.

Because only blasting data on the left side of Jia Hua Tunnel were selected, the left arch foot point (Measuring point B) was on the front-blasting side and the right side arch foot point (Measuring point C) was on the back-blasting side. Therefore, the PPV of the left arch foot was greater than the right. When Section IV was directly above the crown of the Jia Hua Tunnel blasts, the PPV of the left and right arches was nearly identical. When comparing the PPV of the three measuring points in the blasting of Sections I and II, only the horizontal distance of the explosion source

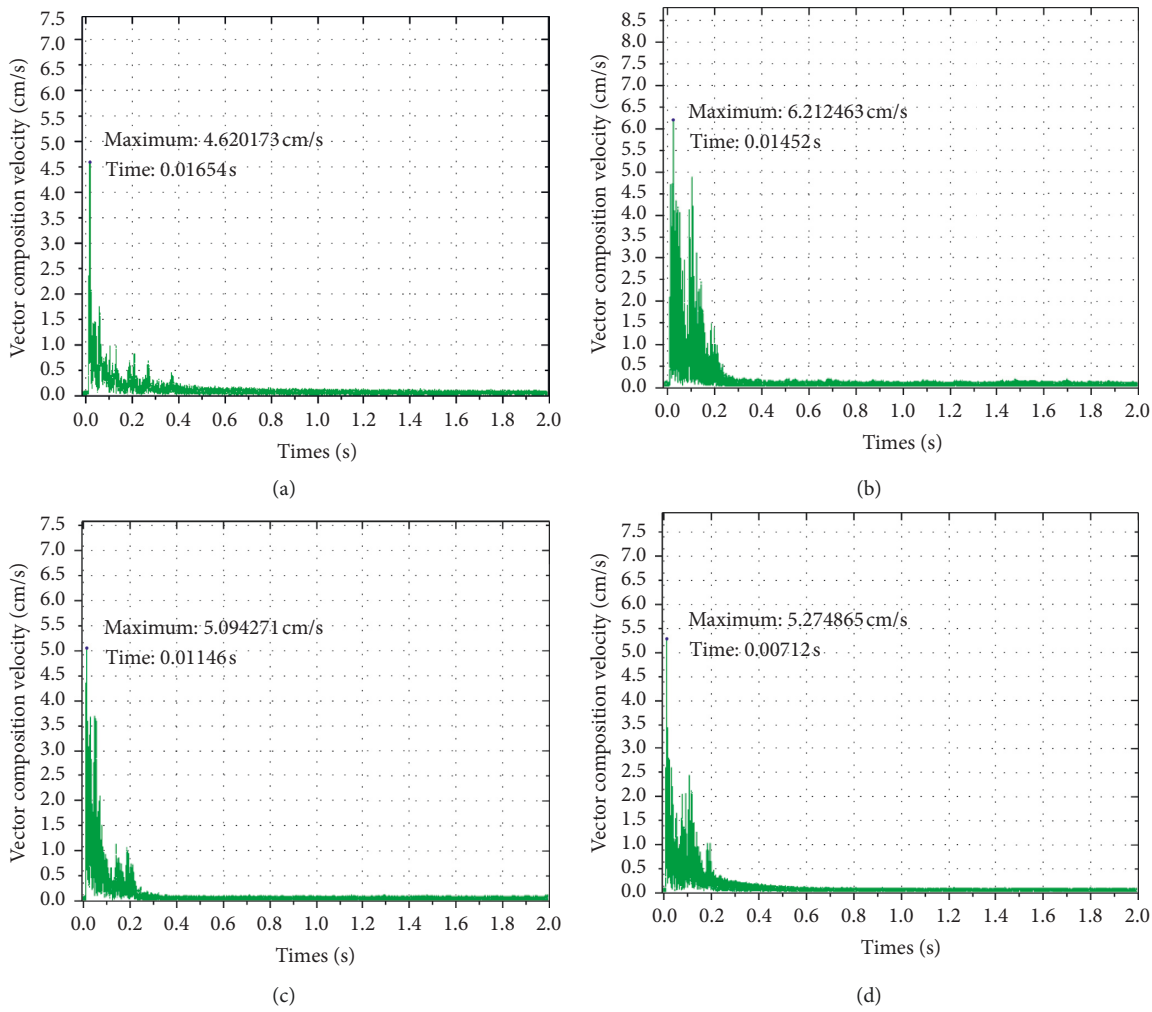

Figure 6: Time-history curve of vibration velocity at Point C during blasting of Section I (a), Section II (b), Section III (c), and Section IV (d).

Table 1: Vibration monitoring data of Jia Hua Tunnel Left Line.

Blasting sections	Blasting cycle footage	Point A		Point B		Point C	
		PPV (cm/s)	Peak acceleration (cm/s^2)	PPV (cm/s)	Peak acceleration (cm/s^2)	PPV (cm/s)	Peak acceleration (cm/s^2)
Section I	1	6.73	38.43	5.22	32.74	4.62	30.97
Section II	1	8.96	62.84	8.05	39.25	6.21	35.90
Section III	0.5	8.25	67.38	6.57	41.57	5.09	41.36
Section IV	0.5	9.48	79.23	5.38	71.75	5.27	42.95

from the measurement point differed. When the blasting method and amount of explosive per delay were identical, the smaller the horizontal distance of the existing tunnel, the larger the blasting vibration.

Comparing the PPV of the three measuring points in the blasting of Sections II and III, the blasting vibration velocity at the same measuring point from Section II to Section III declined. The horizontal distance between Section III and Point A is 1/2 of that of Section II. The blasting cycle footage of Section III was 0.5 m, whereas that of Section II was 1 m. That is, the charge weight in Section III was half that of Section II. Under the influence of blasting vibration in the up-down cross-tunnel, halving the charge weight was better than doubling the horizontal distance damping effect.

Comparing the PPV of the three measuring points in the blasting of Sections III and IV, the blasting vibration velocity at the same measuring point from Section II to Section III decreased. The PPV in Point A of Section IV was greater than that in Section III. At Point A with the same blasting footage, the horizontal distance to Section IV was smaller than Section III. The PPV of Section IV at Point B was also smaller than that of Section III. Point B was directly below Section II, Section III and IV crossed Point B, and Section IV was farther than Section III from Point B. The existing tunnel below was

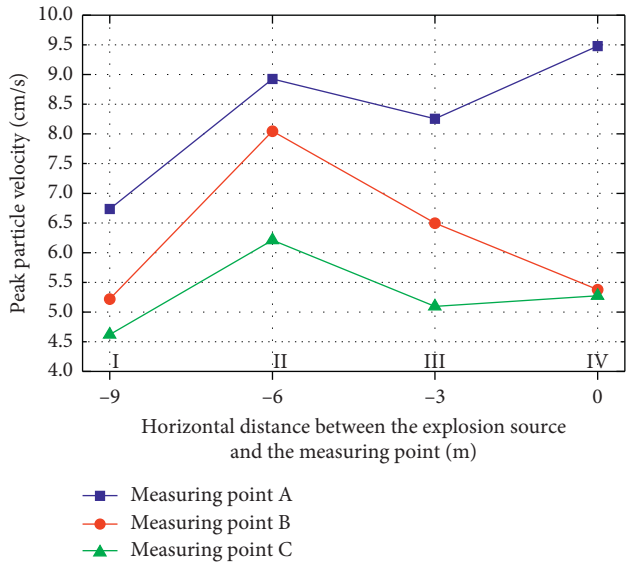

Figure 7: Trends of PPV at Points A, B, and C.

equivalent to a larger damping hole and was more effective in damping Section IV. Therefore, the PPV at Point B declined substantially from Section III to Section IV. The PPV of Section IV at Point C was greater than that of Section III, and the horizontal distance of the Section III was farther than the Section IV from the Point C, and the Point C was located at the right side of the Jia Hua tunnel; the two blasting areas are on the backside, so the farther away from the Section III the damping effect of the Jiahua tunnel is more obvious.

2.4. Monitoring and Analysis of Settlement of Crown in Existing Tunnel. During the tunnel blasting construction, surrounding rock loose areas will be formed around the tunnel. Especially in the construction of small, clear distance cross-tunnels, the loose rock of the excavation tunnel may cause the stress redistribution of the surrounding rock of the existing tunnel, and after the blast disturbance, there will be a secondary subsidence in the existing tunnel. The settlement of the existing tunnel includes the settlement under the initial ground stress and the secondary settlement caused by the upper tunnel blasting disturbance. Furthermore, the settlement of the existing tunnel under the initial ground stress before the upper tunnel blasting excavation has converged. Therefore, the settlement value measured this time is the secondary settlement caused by the blasting excavation of the upper tunnel.

The monitoring points for settlement monitoring at the crown of the Jia Hua Tunnel Left Line were chosen, and K5 + 887.5 mileage was used as the central point for monitoring the settlement value of the existing tunnel below. Along the axis of Jia Hua Tunnel Left Line, the axial mileage increased and decreased in terms of direction, with a monitoring measurement point arranged every 3 m. The specific arrangement is shown in Figure 8.

The value of the crown settlement at each point was monitored once a day continuously until the settlement value of the crown of Jia Hua Tunnel Left Line became stable. The settlement values of each point were recorded and accumulated to plot the cumulative sedimentation values in Figure 9.

Figure 9 shows the accumulated settlement of Jia Hua Tunnel Left Line crown after excavating Gao Jiu Lu I Tunnel. Excavation of the tunnel above the existing tunnel will result in the unloading of the existing tunnel due to the excavation of the soil, which will cause the existing tunnel to have a slight floating condition. However, due to the soft rock mass in the construction area of the project, the blasting excavation has a large disturbance to the surrounding rock mass, and the reconsolidation of the rock mass produces a sinking amount greater than that of the floating, which eventually leads to a slight sinking of the test results of the existing tunnel. The maximum cumulative settlement of the crown of Jia Hua Tunnel Left Line was 18.1 mm at the center of the cross-section of the two tunnels at K5 + 887.5 miles. As the axial distance grew from the center position of the existing tunnel crown, its settlement value gradually declined and convergence accelerated. The area with the largest accumulated settlement value was the cross-section of the new tunnel and the existing tunnel. The distance measurement of the center points was a −4 m to 4 m section. In the vicinity of 24 m from the center point, which was approximately 3 times the new tunnel excavation diameter (the Gao Jiu Lu I Tunnel had a clear width of 8.7 m), the cumulative settlement value changed little. The secondary settlement of the existing tunnel crown due to blasting excavation of the new tunnel was mainly in the cross-section of the two tunnels, and the crown settlement became smaller the farther it moved from the center of the cross-section.

3. Numerical Simulation and Data Analysis

3.1. Calculation Model and Parameters

3.1.1. Models and Boundary Conditions. Finite element calculation of the tunnel structure used the force model of the joint action of the tunnel and stratum. The effect of each construction sequence was simulated and analyzed with regard to the stress and deformation of the stratum and tunnel structure. A three-dimensional finite element model based on the stratigraphy, structural form, and dimensions of the cross-section of Gao Jiu Lu I Tunnel-Jia Hua Tunnel Left Line is shown in Figure 10(a). The size of the model was 50 m in length and width, and the depth from the surface to the bottom of the model was 87.5 m. The four sides of the model limited the horizontal displacement along the normal area to the surface, the bottom limited the displacement in both vertical and horizontal directions, and the top boundary was a free surface. Nonreflective boundary conditions (no reflected waves are generated when seismic waves pass through the boundaries of the model) were applied on the four sides of the model and the ground [22–24], see Figure 10(b) for model meshing details. The model included three parts: stratum, tunnel spray mixing, and tunnel secondary lining. Each part adopted solid elements with the specific model shown in Figure 10(c).

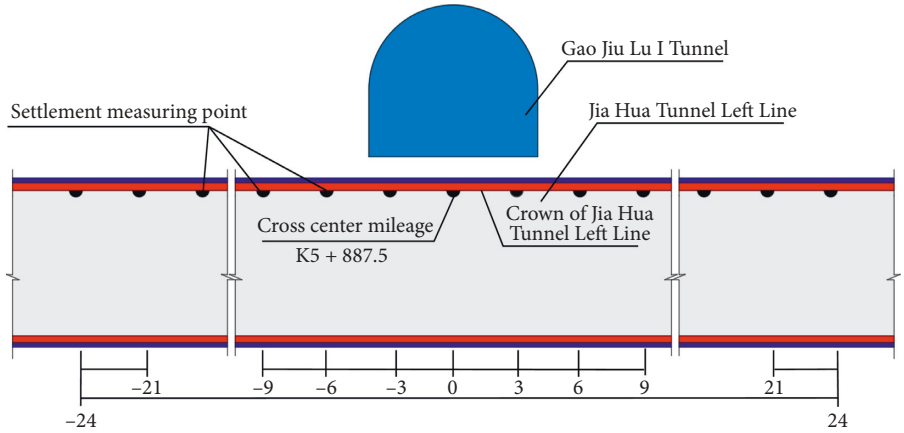

Figure 8: Arrangement of settlement survey points on the Jia Hua Tunnel Left Line crown (unit: m).

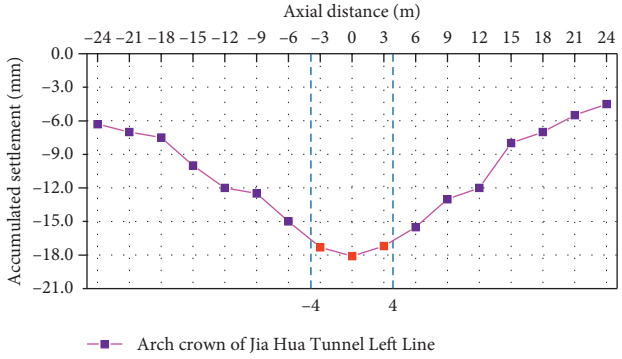

Figure 9: Accumulated settlement of Jia Hua Tunnel Left Line crown.

3.1.2. Calculation Parameters. Shotcrete and formwork concrete are described by the concrete plastic-damage constitutive model that simulates the cracking and crushing of concrete materials. The concrete plastic-damage model can be used to simulate the dynamic loading of blasting loads and has good convergence in the degradation of elastic stiffness caused by tensile and plastic strain [25–27]. The loading function of the concrete plastic-damage constitutive model is

$$F = \frac{1}{1-\alpha}\left[\sqrt{3J_2} + \alpha I_1 + \beta\langle\sigma_{\max}\rangle - \gamma\langle -\sigma_{\max}\rangle\right] - \sigma_{c0}, \tag{1}$$

where I_1 is the first invariant of stress tensor, J_2 is the second invariant of the partial stress tensor, $\sigma_{\max}$ is the maximum eigenvalue of $\overline{\sigma}$, and σ_{c0} is the concrete uniaxial compressive strength.

In formula (1), parameters α, β, and γ are

$$\alpha = \frac{(\sigma_{b0}/\sigma_{c0}) - 1}{2(\sigma_{b0}/\sigma_{c0}) - 1},$$

$$\beta = \frac{\sigma_{c0}}{\sigma_{t0}}(1-\alpha) - (1+\alpha), \tag{2}$$

$$\gamma = \frac{3(1-K_c)}{2K_c - 1},$$

where σ_{b0} is the concrete biaxial compressive strength, σ_{t0} is the concrete uniaxial compressive strength, and K_c is the projection shape parameter that controls the concrete yield surface on the off-plane.

In this paper, for the shotcrete, $K_c = 1.0$ and the projection of the concrete yield surface on the off-plane is circular, similar to the Drucker–Prager criterion in classical elastoplastic theory. For the second lining normal reinforcement concrete, $K_c = 0.67$. The flow rule of the plastic-damage model uses the law of nonassociative flow, and its plastic potential function is

$$G = \sqrt{(\lambda\sigma_{t0}\tan\varphi)^2 + 3J_2} + \sqrt{3}\xi\tan\varphi, \tag{3}$$

where φ is the expansion angle of the concrete yield surface during the strengthening process and λ is the eccentricity of concrete plastic potential function. In this paper, $\varphi = 38°$ and $\lambda = 1.0$ are used.

The physical and mechanical parameters of the surrounding rock and support materials used in the numerical simulation are shown in Table 1 according to the characteristics of geological conditions in the area of the project, geological survey data provided by the surveying unit, and onsite observations. Shotcrete and form concrete were described using a concrete plastic-damage model. Grade IV surrounding rock followed the Mohr–Coulomb yield criterion. All analyses were performed using the finite element software ABAQUS.

In this paper, the classification method of surrounding rock commonly used RMR (rock mass rating) at home and abroad. The rock bulk weight, internal friction angle, and cohesion in Table 2 are the reference values of the grade four surrounding rock according to the "Code for Design of Highway Tunnels" (JIGD70-2004). The elastic modulus of the rock and concrete are determined by multiplying the indoor test standard value of the rock by 0.7. The rock and concrete Poisson's ratio are determined by the indoor test results and references [28, 29].

3.1.3. Simulation Process. Numerical simulation of the cross-section of two tunnels was necessary for the design and

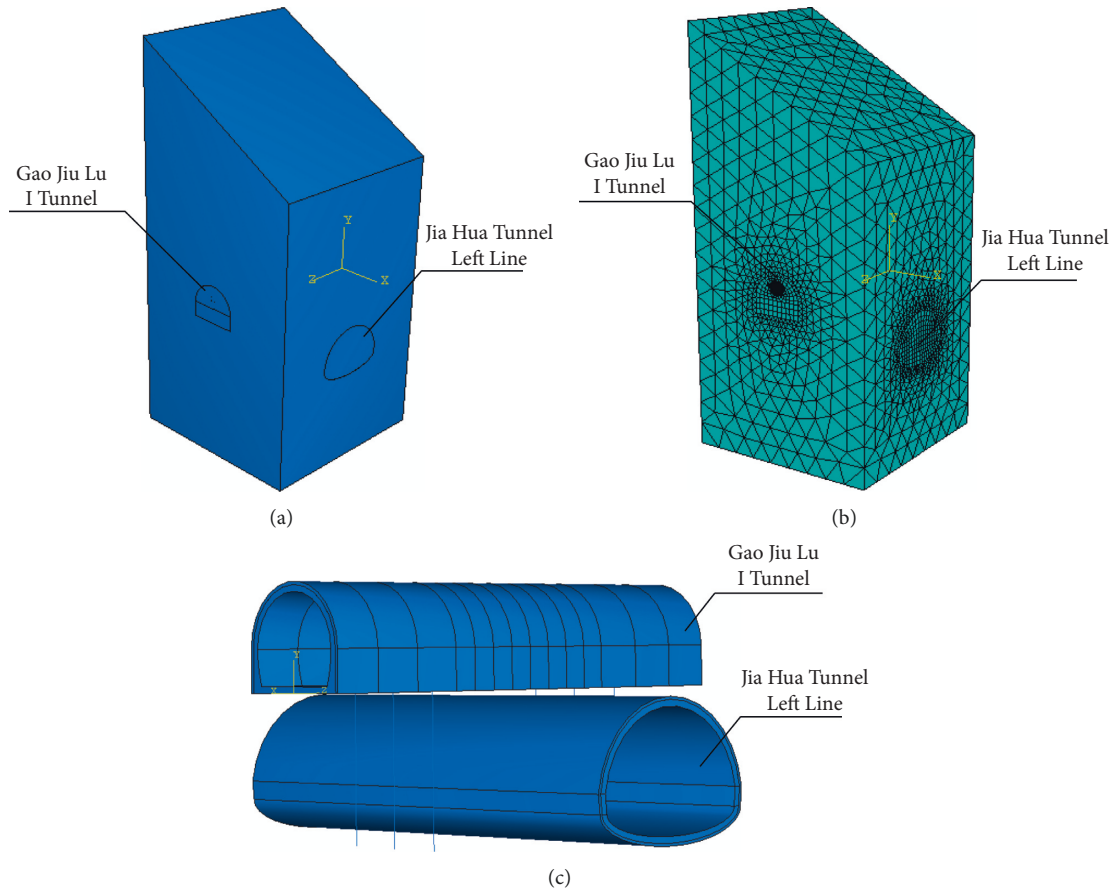

Figure 10: Finite element model: (a) original stratum; (b) meshing; (c) tunnel spray mixing, secondary lining, and pile foundation.

Table 2: Physical and mechanical parameters of finite element calculation.

Medium	Elastic modulus E (GPa)	Poisson's ratio μ	Bulk weight γ (KN/m^3)	Cohesion C (MPa)	Friction angle φ (°)
Grade IV surrounding rock	22.75	0.32	22	0.5	30
C30 formwork concrete	31	0.15	25	2.5	53.8
C30 shotcrete	25	0.15	22	2.5	53.8
Φ25 bolt	200		$D = 2.5$ cm		

optimization of the excavation sequence and support form. ABAQUS provides a rich material model library and cell library, a powerful solver, and unit technology for tunnel excavation simulation. It can simulate the entire tunnel construction process. Due to the large calculation scale, an ABAQUS parallel algorithm based on MPI data exchange technology was adopted based on a comprehensive consideration of the construction, operation process, and calculation capabilities to maximize the actual excavation process. In order to completely simulate the actual site excavation process, the settlement of the existing tunnel vault is caused by the blasting disturbing cloth of the new tunnel above. In the numerical simulation, Jia Hua Tunnel Left Line (the existing tunnel) is first excavated, and the initial ground stress is applied until the settlement of the vault of the existing tunnel is stable, and then the upper section of the Gao Jiu Lu I Tunnel is drilled. The entire analysis was divided into 19 calculation steps as shown in Figure 11.

3.1.4. Blasting Load Application. Blasting construction of the Gao Jiu Lu I Tunnel employed a V-shaped cutting and auxiliary eye and peripheral eye blasting, and the blasting of the cutting hole is the main focus. The layout of the cutting hole is shown in Figure 12. The grooving eye adopts ∅32 mm 2# waterproof emulsion explosive, continuous charging structure, the peripheral eye adopts ∅25 mm 2# waterproof emulsion explosive, air-spaced charge structure, and each blast hole adopts reverse detonation. The blasting sequence was 1-3-5-7-9. When the thickness of the bottom plate is less than 4 m, the total charge weight of blasting per cycle is 6.5 kg and the maximum single-stage charge weight is 0.8 kg. When the thickness of the bottom plate is greater than or equal to 4 m, the total charge weight per blasting is 22.7 kg and the maximum single-stage charge weight is 1.4 kg. The diameter of the blast hole was 40 mm.

The blasting load was simplified as a triangular load with a linear ascending and descending stage. According to tunnel construction and molding requirements, during the

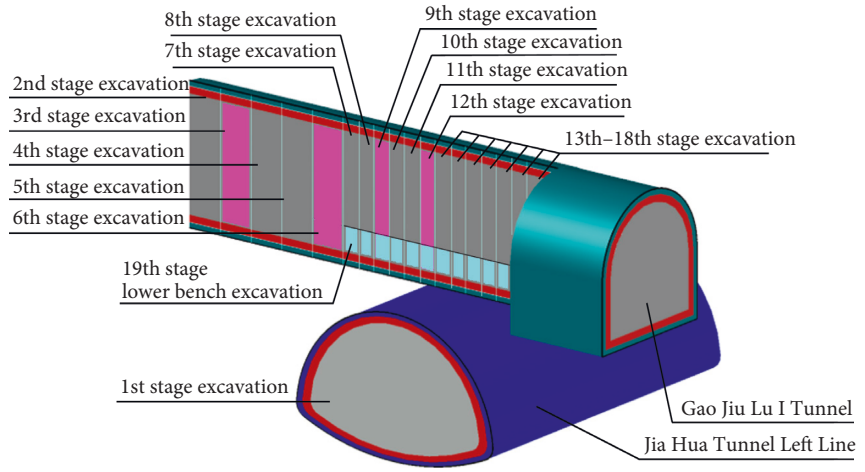

Figure 11: Model simulation excavation process flow chart.

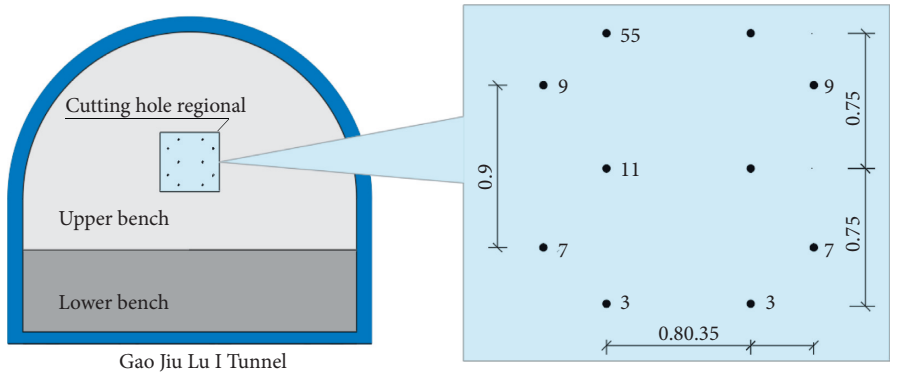

Figure 12: Cutting hole layout (unit: m).

blasting process, the surrounding rock of the tunnel should be protected from damage and the surrounding rock should remain in a state of elastic vibration. Therefore, when establishing the tunnel blasting vibration model, the following assumptions apply: (1) the blasting vibration load acts on the circumferential wall of the tunnel in the form of uniform pressure load, and the direction of action is normal; (2) the surrounding wall of the tunnel is in the far zone of blasting, and the blasting vibration load of the surrounding wall of the tunnel will not cause damage to the surrounding rock; and (3) the blasting vibration load is simplified as a triangular load. The value of the peak stress load of the blasting load is related to the type of surrounding rock, type of explosive, blast hole arrangement, and maximum charge weight.

The calculation of the burst pressure generated per 1 kg of explosive is calculated using the formula proposed by the National Highway Institute (US, 1991):

$$P_{\text{det}} = \frac{4.18 \times 10^{-7} \times \text{sge} \times V_e^2}{1 + 0.8\,\text{sge}}. \tag{4}$$

The pressure on the wall of the hole is based on the following formula:

$$P_B = P_{\text{det}} \times \left(\frac{d_c}{d_h}\right)^3, \tag{5}$$

where P_{det} is the burst pressure (KPa), P_B is the pressure on the wall of the hole (KPa), V_e is the blasting speed (m/s), d_c is the roll diameter (mm), d_h is the eyelet diameter (mm), and sge is the explosive weight (g/cm^3).

The above formula can be used to determine the amount of aerodynamic pressure generated during an explosion. The time-dependent dynamic pressure function acting on the wall of the hole in actual engineering can be calculated by the window function formula proposed by Starfield and Pugliese (1968):

$$P_D(t) = 4P_B\left(\exp\left(\frac{-Bt}{\sqrt{2}}\right) - \exp\left(-\sqrt{2}\,Bt\right)\right), \tag{6}$$

where B is the blasting constant, dynamic pressure per 1 kg charge, $B = 16338$.

The total time for calculating the triangular pulse load was 100 ms, including a rise time of 10 ms, fall time of 90 ms, and peak pressure of 0.375 MPa.

3.2. Analysis of Simulation Results

3.2.1. Analysis of Vibration Calculation Results. To calculate the model of the second lining surface of Jia Hua Tunnel, three particle points corresponding to actual measurement Points A, B, and C were selected as measurement points. The #1 measuring point of the second lining crown of Jia Hua

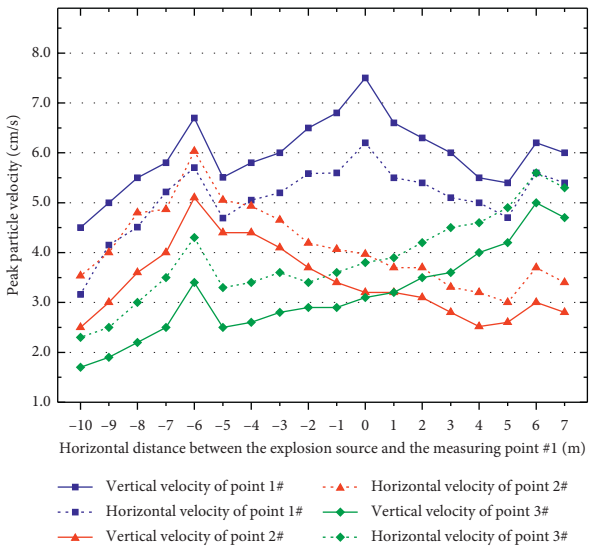

Figure 13: Trends in PPV of #1, #2, and #3 measuring points.

Tunnel Left Line, #2 measuring point of the left arch foot, and #3 measuring point of the right arch foot were, respectively, chosen. The calculated three peak vibration velocities were the horizontal velocity along the Jia Hua tunnel axis, the horizontal velocity along the radial direction of the Jia Hua tunnel, and the vertical velocity in the vertical direction. The peak velocity of particles in the three observation directions for the same measurement point was different. The more consistent the observation direction was with the normal direction of the wave front propagated by the seismic wave, the higher the vibration velocity. The Gao Jiu Lu I Tunnel axis was nearly perpendicular to Jia Hua Tunnel Left Line axis. The horizontal radial direction was more consistent with the horizontal axis direction and the wave front normal direction. Therefore, the horizontal radial direction vibration speed was greater than that of the horizontal axis direction. To facilitate data processing, a large horizontal radial vibration velocity and vertical vibration velocity were selected for analysis. The horizontal radial peak vibration velocity and vertical peak vibration velocity generated by each calculation step are plotted in Figure 13.

Figure 13 displays the following: (1) The vertical PPV of the #1 measuring point of the crown was substantially larger than the horizontal PPV. The horizontal vibration velocity of measuring points #2 and #3 of the arch was substantially larger than the vertical PPV. That is, the vibration velocity of the particle exhibited a clear direction effect, and the vibration velocity of the particle toward the empty surface was clearly greater than in other directions. The crown mainly manifested as up-and-down vibrations, whereas the arch foot mainly exhibited horizontal vibrations. The vertical PPV of #1 measuring point of Jia Hua Tunnel Left Line crown was highest. Despite that the horizontal distance from the source to the measuring point was 0, the vertical PPV of the measuring point reached 7.53 cm/s and the other vertical PPV did not exceed 7 cm/s. The second line of Jia Hua Tunnel Left Line was not unstable from blasting. (2) The change trend of the PPV at each measurement point and the horizontal distance from the explosion source to the measurement point were well aligned. According to the arrangement of the measuring points of the tunnel, the distance between the three measuring points and the explosion source proceeded from far to near to far. The PPV of the corresponding measuring point proceeded from small to large to small. The PPV of each measuring point did not appear in the same blasting operation. With a decline in the horizontal distance from the source to the measuring point, the #2 measuring point showed the first peak, followed by the #1 measuring point and finally the #3 measuring point. (3) The PPV velocity curve can be roughly divided into four phases: The horizontal distance of the explosion source from the measuring point was −10 to −6 m for the first stage. That is, the 1.0 m phase of the I-track tunnel blasting cycle showed a relatively small PPV overall and increased as the horizontal distance decreased. The horizontal distance from the explosion source to the measurement point was −6 to −5 m for the second stage; thus, the blasting cycle footage was reduced to a 0.5 m blasting stage, at which time the blasting vibration velocity was reduced substantially. The horizontal distance of the explosion source from the measuring point was −5 to 5 m, marking the third stage. The particle vibration speed was higher at the crossing stage. As the horizontal distance changed from far to near to far, the gradual increase in vibration speed peaked and then began to fall, indicating the key control phase. The horizontal distance from the source to the measuring point was 5–7 m for the fourth stage, and the excavation tunnel had passed through the existing tunnel cross-section. The symmetrical distribution of the PPV at the measuring point and the overall PPV indicated that when the cycle footage increased, the PPV rose and then began to decay. The attenuation trend of each measurement point was similar at the second phase.

3.2.2. Stress Calculation Results. Figure 14 presents the initial stress distribution map of the cross-section. Before tunnel excavation, the three directions of the stress component in the area were distributed in layers. Deep in the stratum, the isosurface was essentially parallel to the horizontal plane; near the surface, the isosurface tended to develop parallel to the ground surface. The initial ground stress field obtained by this model was reasonable, and the model establishment was reliable.

The main stress cloud map of the secondary lining of Jia Hua Tunnel Left Line in Figure 15 shows that the maximum tensile stress of the secondary lining was mainly concentrated in the crown area. The maximum tensile stress was only 0.005 MPa, far less than the tensile strength of the concrete. The maximum compressive stress was concentrated in the arch foot area. The maximum compressive stress was only 0.15 MPa, far below the compressive strength of concrete. Thus, the upper part of the tunnel was mainly supported by surrounding rock and initial support, and the secondary lining was safe. If the load reached the breaking strength of concrete, then the tunnel secondary lining at the

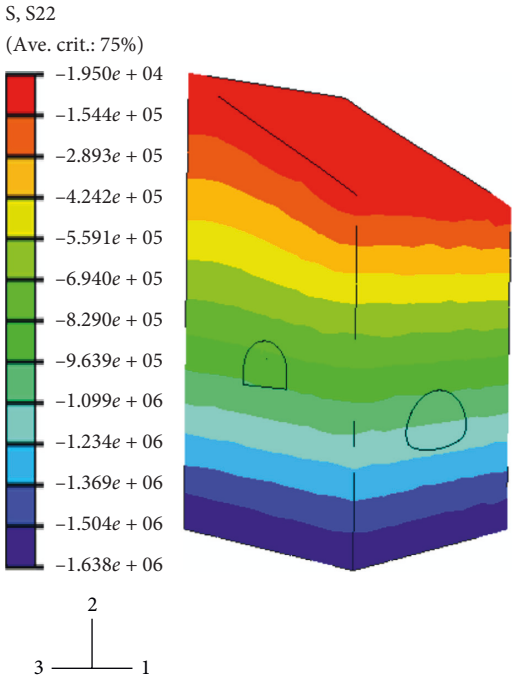

Figure 14: Model of initial ground stress (unit: Pa).

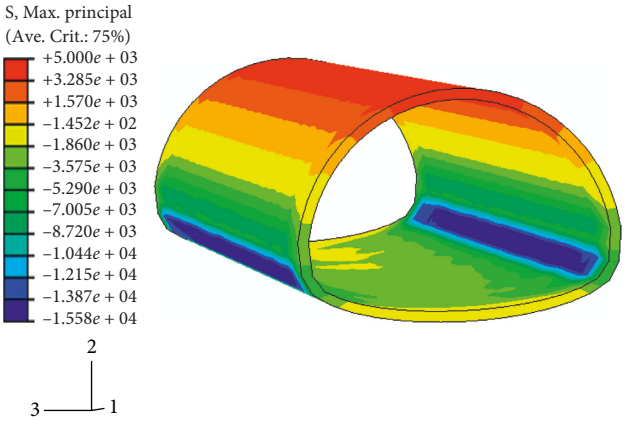

Figure 15: Main stress cloud diagram of secondary lining of Jia Hua Tunnel Left Line (unit: Pa).

arch foot would be stretched and then shear pressure would break.

3.2.3. Analysis of Settlement Calculation Results. After excavating the Gao Jiu Lu I Tunnel, the maximum settlement around Jia Hua Tunnel Left Line occurred near the crown. The tunnel arch bottom exhibited a lifting tendency and a maximum upward displacement of 0.4 mm as shown in Figure 16(a). The vertical displacement map displayed a linear pattern with less regularity, and the seismic wave was gradually transmitted to the left and right boundaries far from the tunnel. Changes in the surface of the earth appeared to vary greatly due to the peaks and valleys of seismic waves. The maximum values alternated between the upper and lower ends of the tunnel.

As can be seen from Figure 16(b), the settlement of the two tunnel concrete support systems was mainly concentrated in the lining crown at the cross-section of the two tunnels. The Gao Jiu Lu I Tunnel showed a mixing crown maximum settlement of 25 mm. The maximum settlement of Jia Hua Tunnel Left Line was 17.3 mm. The settlement value along the axial direction of the tunnel declined gradually, the settlement trend tended to be gentle, and the settlement convergence speed accelerated.

4. Discussion

Figure 17 presents the horizontal and the vertical vibration velocity vector of the #1, #2, and #3 measurement points in Jia Hua Tunnel Left Line of the numerical simulation along

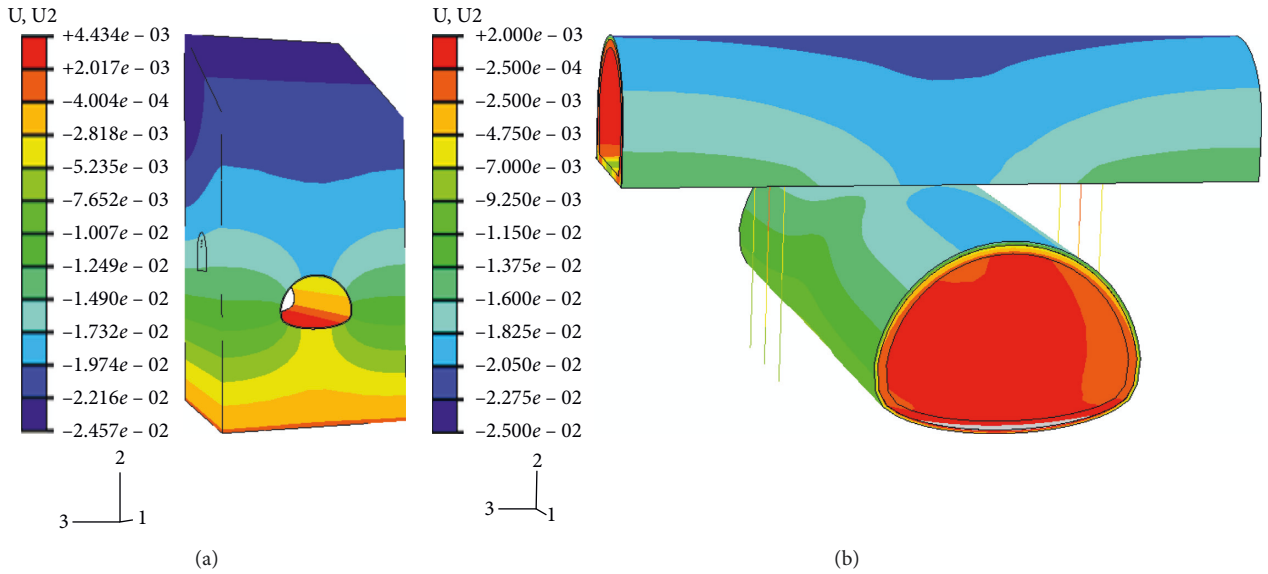

Figure 16: Vertical displacement distribution of Jia Hua Tunnel Left Line (unit: m).

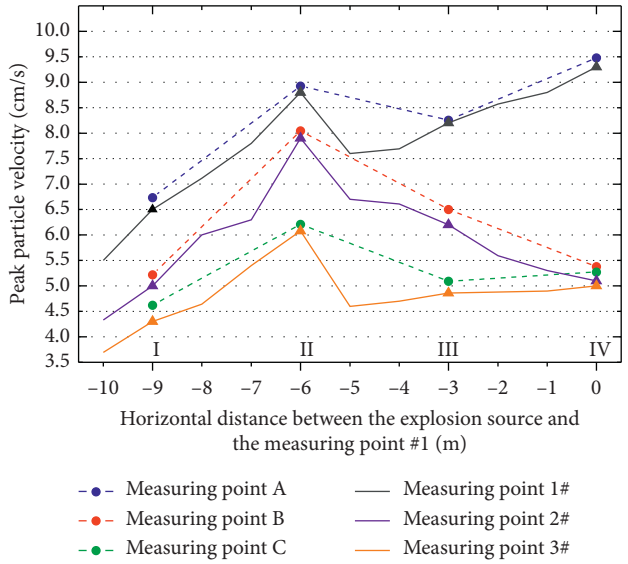

Figure 17: Comparison of PPV between onsite measurements and simulations on Jia Hua Tunnel Left Line.

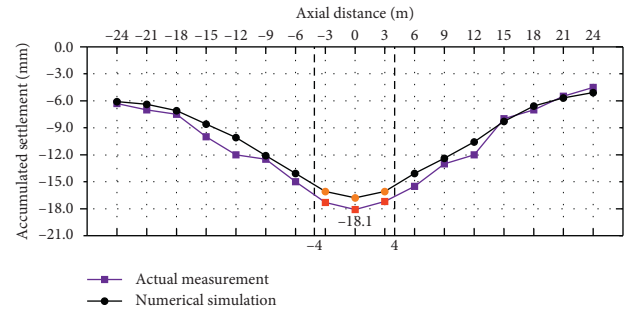

Figure 18: Cumulative settlement curve of vaults in Jia Hua Tunnel Left Line.

with the vector synthesis PPV of the measured Points A, B, and C in the blasting excavation process.

As can be seen from Figure 17, in the numerical simulation, the horizontal distance of the blast source from measuring points −9, −6, −3, and 0 m corresponded to Sections I, II, III, and IV of the onsite measured data, respectively. The measured PPV of the four sections was largely consistent with the PPV at the corresponding stages of the numerical simulation. The change trend showed good correspondence, suggesting that the numerical simulation better reflected the actual blasting process, and the established model was correct and reliable. Measured Point A and numerical simulation of the #1 measuring point during the entire blasting process showed the maximum PPV, the position where the new tunnel demonstrated the greatest blasting vibration influence on the crown of the existing tunnel below in the cross-section. The blasting vibration in the up-down cross-tunnel was smaller with an increase in the horizontal distance of the explosion source. The closer to the source of the explosion, the more intense the vibration. The vibration also conformed to the general blasting vibration law. The measured data of Sections II and III concurred well with the numerical simulations of the −6 m and −3 m calculation steps. The PPV of Section II at the same point was less than that of Section III, implying that when the horizontal distance was less than 1 time the diameter of the existing tunnel below the blasting vibration influence of a small, clear distance up-down cross-tunnel, reducing the doubled charge weight was better than doubling the horizontal distance. Compared with Sections III and IV, the PPV of the crown from −3 m to 0 m increased; however, the amplitude of the vibration of the arch foot measuring point under the two explosions was clearly reduced. The existing tunnel below had a certain damping effect on its own arch foot and arch bottom. The insufficiency of research on the influence of blasting vibration has included no quantitative analysis of the relationship between the horizontal distance of the existing tunnel below the explosive source distance

and the explosive charge, nor has research provided further derivation of the quantitative analysis of the damping effect of the existing tunnel below.

Figure 18 shows the cumulative settlement values of Jia Hua Tunnel Left Line crown measured during numerical simulation and blasting excavation. A comprehensive analysis of Figure 18 shows that the trend of the cumulative settlement values of the crown onsite measured and numerical simulation points were nearly the same. The maximum settlement of Jia Hua Tunnel Left Line was measured to be 18.1 mm, directly below the cross-section. Numerical simulation showed the maximum settlement around Jia Hua Tunnel Left Line near the crown, and its settlement value was 17.8 mm. The maximum difference between the measured and numerical simulation was 3 mm, within the acceptable error range. The farther away from the center of the cross-section, the smaller the difference. The trend of the two curves indicates that the cumulative settlement value of the existing tunnel crown declined gradually as the axial distance from the crossed section center increased. The value became stable approximately 24 m away from the cross-center. That is, the settlement value of the cross-section was affected by the blasting vibration more than the influence of the uncrossed section. The above comparative analysis indicates that during the construction of blasting similar to the up-down cross-tunnels in the future, the support for the crown of the existing tunnel below was reinforced on both sides of the crosscenter within a diameter of 3 times the new tunnel, thereby ensuring existing tunnel safety.

5. Conclusion

In this paper, a blasting excavation of the Gao Jiu Lu I Tunnel was carried out along with a blasting vibration and crown settlement of Jia Hua Tunnel Left Line below. The influence of Gao Jiu Lu I Tunnel blasting on Jia Hua Tunnel Left Line below was analyzed using a finite element simulation construction excavation process. The influence of the blasting excavation of the new tunnel on the existing tunnel below was found in the tunnel with a small clear distance up and down. This paper mainly analyzed the vibration velocity, stress, and displacement of the secondary lining of the existing tunnel below. The following conclusions were drawn from this study:

(1) The peak vibration velocity and peak acceleration at the vault of the second lining of the existing tunnel below are the greatest when the small, clear distance cross-tunnel blasting excavation. The new tunnel exerted the greatest impact on the blasting vibration of the existing tunnel below at the crown of the existing tunnel below at the cross-section. When the horizontal distance from the existing tunnel below the explosion source was less than 1 times the diameter of the existing tunnel below, the peak vibration velocity can be reduced better by reducing the doubling of explosive charge than by doubling the horizontal distance. The vibration of the second lining of the existing tunnel has obvious directional effect. The vibration velocity of the particle toward the free surface is obviously greater than that in other directions. The vault mainly shows up-and-down vibration, while the arch foot mainly shows horizontal vibration.

(2) The redistribution of stress in surrounding rock caused by blasting excavation of the new tunnel above leads to that the maximum tensile stress of secondary lining of existing tunnel below was mainly concentrated in the crown area, and the value was far less than the tensile strength of concrete at that point. The maximum compressive stress was concentrated in the arch foot area, and its value was much smaller than the concrete compressive strength.

(3) The effect of the new tunnel on the settlement of the existing tunnel below was primarily evidenced by loosening of the surrounding rock caused by blasting excavation in the new tunnel, which resulted in secondary settlement of the existing tunnel below the crown and the maximum accumulated settlement value at the cross-section of the two tunnels. With an increase in axial distance between the existing tunnel crown and the cross-section, the settlement value gradually declined and became stable.

Data Availability

The data used to support the findings of this study are available from the corresponding author upon request.

Conflicts of Interest

The authors declare that they have no conflicts of interest.

Acknowledgments

This paper was supported by the National Natural Science Foundation of China (no. 51704183).

References

[1] J.-H. Shin, H.-G. Moon, and S.-E. Chae, "Effect of blast-induced vibration on existing tunnels in soft rocks," *Tunnelling and Underground Space Technology*, vol. 26, no. 1, pp. 51–61, 2011.

[2] B. Duan, H. Xia, and X. Yang, "Impacts of bench blasting vibration on the stability of the surrounding rock masses of roadways," *Tunnelling and Underground Space Technology*, vol. 71, pp. 605–622, 2018.

[3] C. W. W. Ng, T. Boonyarak, and D. Mašín, "Three-dimensional centrifuge and numerical modeling of the interaction between perpendicularly crossing tunnels," *Canadian Geotechnical Journal*, vol. 50, no. 9, pp. 935–946, 2013.

[4] H. Mohamad, P. J. Bennett, K. Soga, R. J. Mair, and K. Bowers, "Behaviour of an old masonry tunnel due to tunnelling-induced ground settlement," *Géotechnique*, vol. 60, no. 12, pp. 927–938, 2015.

[5] H. Chakeri, R. Hasanpour, M. A. Hindistan, and B. Ünver, "Analysis of interaction between tunnels in soft ground by 3D

numerical modeling," *Bulletin of Engineering Geology and the Environment*, vol. 70, no. 3, pp. 439–448, 2011.

[6] J. C. Li, H. B. Li, G. W. Ma, and Y. X. Zhou, "Assessment of underground tunnel stability to adjacent tunnel explosion," *Tunnelling and Underground Space Technology*, vol. 35, pp. 227–234, 2013.

[7] H.-b. Zhao, Y. Long, X.-h. Li, and L. Lu, "Experimental and numerical investigation of the effect of blast-induced vibration from adjacent tunnel on existing tunnel," *KSCE Journal of Civil Engineering*, vol. 20, no. 1, pp. 431–439, 2016.

[8] M. Chen, W. B. Lu, P. Yan, and Y. G. Hu, "Blasting excavation induced damage of surrounding rock masses in deep-buried tunnels," *KSCE Journal of Civil Engineering*, vol. 20, no. 2, pp. 933–942, 2016.

[9] X. Li, W. Cao, M. Tao, Z. Zhou, and Z. Chen, "Influence of unloading disturbance on adjacent tunnels," *International Journal of Rock Mechanics and Mining Sciences*, vol. 84, pp. 10–24, 2016.

[10] Q. Liang, J. Li, D. Li, and E. Ou, "Effect of blast-induced vibration from new railway tunnel on existing adjacent railway tunnel in Xinjiang, China," *Rock Mechanics and Rock Engineering*, vol. 46, no. 1, pp. 19–39, 2013.

[11] X. Li, Y. Long, and C. Ji, "Study on the vibration effect on operation subway induced by blasting of an adjacent cross tunnel and the reducing vibration techniques," *Journal of Vibroengineering*, vol. 15, no. 3, pp. 1454–1462, 2013.

[12] F. Yang, S. Cao, and G. Qin, "Performance of the prestressed composite lining of a tunnel: case study of the yellow river crossing tunnel," *International Journal of Civil Engineering*, vol. 16, no. 2, pp. 229–241, 2018.

[13] V. R. Feldgun, Y. S. Karinski, and D. Z. Yankelevsky, "The effect of an explosion in a tunnel on a neighboring buried structure," *Tunnelling and Underground Space Technology*, vol. 44, pp. 42–55, 2014.

[14] X. Xia, H. B. Li, J. C. Li, B. Liu, and C. Yu, "A case study on rock damage prediction and control method for underground tunnels subjected to adjacent excavation blasting," *Tunnelling and Underground Space Technology*, vol. 35, pp. 1–7, 2013.

[15] R. Liang, T. Xia, Y. Hong, and F. Yu, "Effects of above-crossing tunnelling on the existing shield tunnels," *Tunnelling and Underground Space Technology*, vol. 58, pp. 159–176, 2016.

[16] X. L. Jiang, F. F. Wang, H. Yang, and J. Y. Niu, "Parameter sensitivity of shallow-bias tunnel with a clear distance located in rock," *Advances in Civil Engineering*, vol. 2018, Article ID 5791354, 11 pages, 2018.

[17] M. Z. Emad, H. Mitri, and C. Kelly, "Dynamic model validation using blast vibration monitoring in mine backfill," *International Journal of Rock Mechanics and Mining Sciences*, vol. 107, pp. 48–54, 2018.

[18] N. Jiang and C. Zhou, "Blasting vibration safety criterion for a tunnel liner structure," *Tunnelling and Underground Space Technology*, vol. 32, pp. 52–57, 2012.

[19] J. Lai, H. Fan, J. Chen, J. Qiu, and K. Wang, "Blasting vibration monitoring of undercrossing railway tunnel using wireless sensor network," *International Journal of Distributed Sensor Networks*, vol. 11, no. 6, pp. 1550–1329, 2015.

[20] Z. Kaláb, B. Pandula, M. Stolárik, and J. Kondela, "Examples of law of seismic wave attenuation," *Metalurgija -Sisak then Zagreb*, vol. 52, no. 3, pp. 387–390, 2013.

[21] Y. T. Zhao, C. Chu, A. Vafeidis, and J. Li, "Vibration of a cylindrical tunnel under a centric point-source explosion," *Shock and Vibration*, vol. 2017, Article ID 9152632, 7 pages, 2017.

[22] C. W. W. Ng, K. Y. Fong, and H. L. Liu, "The effects of existing horseshoe-shaped tunnel sizes on circular crossing tunnel interactions: three-dimensional numerical analyses," *Tunnelling and Underground Space Technology*, vol. 77, pp. 68–79, 2018.

[23] D. Uystepruyst and F. Monnoyer, "A numerical study of the evolution of the blast wave shape in rectangular tunnels," *Journal of Loss Prevention in the Process Industries*, vol. 34, pp. 225–231, 2015.

[24] J. X. Zhou, Y. Luo, X. P. Li, Y. H. Guo, and T. T. Liu, "Numerical evaluation on dynamic response of existing underlying tunnel induced by blasting excavation of a subway tunnel," *Shock and Vibration*, vol. 2017, Article ID 8628671, 10 pages, 2017.

[25] G. F. Zhao, J. K. Xu, Y. L. Li, and M. Zhang, "Numerical analysis of the degradation characteristics of bearing capacity of a corroded reinforced concrete beam," *Advances in Civil Engineering*, vol. 2018, Article ID 2492350, 10 pages, 2018.

[26] Y. Chi, M. Yu, L. Huang, and L. Xu, "Finite element modeling of steel-polypropylene hybrid fiber reinforced concrete using modified concrete damaged plasticity," *Engineering Structures*, vol. 148, pp. 23–35, 2017.

[27] T. Yu, J. G. Teng, Y. L. Wong, and S. L. Dong, "Finite element modeling of confined concrete-II: plastic-damage model," *Engineering Structures*, vol. 32, no. 3, pp. 680–691, 2010.

[28] X.-X. Yang and W.-G. Qiao, "Numerical investigation of the shear behavior of granite materials containing discontinuous joints by utilizing the flat-joint model," *Computers and Geotechnics*, vol. 104, pp. 69–80, 2018.

[29] J. Hu, S. Li, L. Li et al., "Field, experimental, and numerical investigation of a rockfall above a tunnel portal in southwestern China," *Bulletin of Engineering Geology and the Environment*, vol. 77, no. 4, pp. 1365–1382, 2018.